COBEM 2023 27TH INTERNATIONAL CONGRESS OF MECHANICAL ENGINEERING

ABCM Brazilian Society of Mechanical Sciences and Engineering
27th ABCM International Congress of Mechanical Engineering
December 04-08, 2023, Florianópolis-SC, Brazil

COB-2023-2316
SYMMETRICAL DAMAGE DETECTION IN BEAM STRUCTURES USING WAVE PROPAGATION AND PIEZOELECTRIC SENSORS A THEORETICAL STUDY

Pedro Christian Ayala Castillo
Department of Mechanical Engineering, UNIFESSPA, Marabá, Pará, Brazil
Pedro.ayala@unifesspa.edu.br

Michael John Brennan
Department of Mechanical Engineering, UNESP-FEB, Bauru, São Paulo, 17033-360, Brazil

Bing Tang
Institute of Internal Combustion Engine, Dalian University of Technology, Dalian 1160023, China

Abstract. *Structural Health Monitoring (SHM) has gained significant attention for early detection of damage in structures through wave propagation research. This paper presents a theoretical study of wave propagation for the purpose of detecting and quantifying damage in beam structures, with a specific focus on the interaction of waves with symmetrical damage relative to the neutral axis. An analysis of a one-dimensional structural waveguide with a piezoelectric actuator and sensors in pitch-catch and pulse-echo configurations is presented. The model is developed in the frequency domain and transformed into the time domain using the inverse Fourier transform, allowing investigation of the effect of damage on wave propagation in both domains. The size of the actuator, sensor, and damage is studied for a thin aluminum beam. Results show that the time-domain approach is preferable over a frequency-domain approach for damage detection in this type of structure. Longitudinal waves are found to be more sensitive to changes in thickness for symmetrical systems, and measuring reflected waves is more effective than transmitted waves. The findings also reveal that the dispersive nature of bending waves can result in decreased reflected wave amplitude with reduced beam thickness in certain situations.*

Keywords: *Damage detection, structural health monitoring, wave propagation.*

1. INTRODUCTION

In recent years the use of wave propagation for Structural Health Monitoring (SHM) has been of increasing interest and is the subject of this paper. The aim of SHM is to detect damage in its early stage of development. High frequency waves are generated that interact with the damage, and the way in which the wave changes as it interacts with the damage, is used to detect the damage (Ostachowicz et al., 2012). Many structures have components made of beams and bars, which have a uniform cross-section with homogeneous physical and geometric properties. It is the detection and quantification of damage in such structures that are investigated in this paper.

The importance of the use of the wave propagation approach was described by Tenenbaum et al. (2011), who carried out a comparison of vibration and wave propagation approaches to assess damage in Euler-Bernoulli beams. Their results with different damage scenarios, showed that the vibrational approach has the advantage of being directly applicable in more complex structures. Otherwise, the wave approach has a significant economy of time and computational effort.

Early work by Mace (1984) discussed the vibrational behaviour of the beam systems in terms of wave propagation. He wrote down the relationships between wave amplitudes at various positions on the beam, and emphasized the importance of nearfield waves close to discontinuities. Models developed by (1990), and Wang and Rogers (1991) on piezoelectric (PZT) actuators were used by Brennan (1994), in the active control of wave motion in beams. These models are used in this paper to couple PZT actuators to the beam. The models are also modified to characterize damage in a Euler-Bernoulli Beam. The limitation of the Euler Bernoulli beam model is that it can provide an accurate result only when the ratio of wavelength to thickness is greater than 6 (Fahy; Gardonio, 2007).

This paper is organized as follows. In section 2 wave propagation theory is briefly reviewed. In section 3 a longitudinal or flexural wave are considered to interact with the damage. The way in which these generate transmitted and reflected waves is studied. The optimal sizes of sensor and actuator for a specific frequency are determined in Section 4 before the complete system is analyzed in the time domain in section 5.

2. WAVE PROPAGATION IN BARS AND BEAMS

Wave propagation involves the transport of energy in space and time. This contrasts with vibrations that set each point in the structure in motion simultaneously (Doyle, 2009).

The axial displacement $u(x,t)$ of a bar for free wave motion is governed by the partial differential equation (Graff, 1975)

$$ES\frac{\partial^2 u}{\partial x^2} - \rho S\frac{\partial^2 u}{\partial t^2} = 0\,, \tag{1}$$

where E is the modulus of elasticity, S is the cross-sectional area and ρ is the density of the bar. It is assumed that the vibration of the structure is linear and time-harmonic. This last assumption allows $\exp(+\mathrm{j}\omega t)$ time dependency to be suppressed for clarity. The general solution of equation **Erro! Fonte de referência não encontrada.** for in-plane displacement is given by

$$u(x) = A_r \exp(-\mathrm{j}k_l x) + A_l \exp(+\mathrm{j}k_l x)\,, \tag{2}$$

where A_l and A_r are the amplitude of the left- and right-going propagating longitudinal waves respectively, ω is the circular frequency, $\mathrm{j}=\sqrt{-1}$, and $k_l = 2\pi/\lambda_l$ is the longitudinal wave number in which λ_l is the longitudinal wavelength.

The transverse displacement $w(x,t)$ of the beam for free wave motion is governed by the partial differential equation (Graff, 1975)

$$EI\frac{\partial^4 w}{\partial x^4} - \rho S\frac{\partial^2 w}{\partial t^2} = 0\,, \tag{3}$$

where I is the second moment of area, which for a rectangular beam is given by $I = bh^3/12$ where b is the breadth and h is the depth of the beam respectively. It is assumed, as in the same case of longitudinal waves, that the vibration of the structure is linear and time-harmonic. The general solution of equation (3) for the out-of-plane displacement is given by

$$w(x) = A_1 \exp(+k_f x) + A_2 \exp(-k_f x) + A_3 \exp(+\mathrm{j}k_f x) + A_4 \exp(-\mathrm{j}k_f x)\,, \tag{4}$$

where A_3 and A_4 are the amplitudes of the left- and right-going flexural propagating flexural waves respectively, A_1 and A_2 are the left- and right-going amplitude evanescent or near-field waves respectively, and $k_f = 2\pi/\lambda_f$ is the flexural wavenumber in which λ_f is the flexural wavelength.

3. MODELLING SYMMETRIC DAMAGE

The approach used by Brennan et al. (1997) is used to model the beam, in which uniform sections of the beam are modelled as waveguides being represented by simple transmission matrices. The part of the beam with the reduced section (the damaged part) is considered as another uniform element. The state-vectors are obtained for each side of the damage to connect the damaged part of the beam to the other sections. The relationship between the state-vector and the waves on the beam in a junction is given by

$$\begin{Bmatrix} u \\ w \\ \theta \\ M \\ Q \\ F \end{Bmatrix} = \begin{Bmatrix} u \\ w \\ w' \\ EIw'' \\ EIw''' \\ ESu' \end{Bmatrix} = \begin{bmatrix} 0 & 0 & 1 & 0 & 0 & 1 \\ 1 & 1 & 0 & 1 & 1 & 0 \\ k_f & \mathrm{j}k_f & 0 & -k_f & -\mathrm{j}k_f & 0 \\ EIk_f^2 & -EIk_f^2 & 0 & EIk_f^2 & -EIk_f^2 & 0 \\ EIk_f^3 & -\mathrm{j}EIk_f^3 & 0 & -EIk_f^3 & \mathrm{j}EIk_f^3 & 0 \\ 0 & 0 & \mathrm{j}ESk_l & 0 & 0 & -\mathrm{j}ESk_l \end{bmatrix} \begin{Bmatrix} A_1 \\ A_3 \\ A_l \\ A_2 \\ A_4 \\ A_r \end{Bmatrix}, \tag{5}$$

where $'$ denotes the spatial derivate with respect to x, θ is the beam rotation, M is the internal bending moment, Q is the out-of-plane force and F the in-plane force.

Equation (5) can be written for the junctions of the beam either side of the damage as

$$\mathbf{h}_B^L = \mathbf{H}_B \mathbf{a}_B^L, \tag{6}$$

and

$$\mathbf{h}_B^R = \mathbf{H}_B \mathbf{a}_B^R, \tag{7}$$

where $\mathbf{h}_B$ is the state vector, $\mathbf{H}_B$ is the transformation matrix and $\mathbf{a}_B$ is the vector of waves, the subscript B indicates that the variable belongs to the beam without damage and the superscripts L and R denote the left- and right-hand junctions. The two junctions of the beam with damage are given by

$$\mathbf{h}_D^L = \mathbf{H}_D \mathbf{a}_D^L, \tag{8}$$

and

$$\mathbf{h}_D^R = \mathbf{H}_D \mathbf{a}_D^R, \tag{9}$$

where the subscript D denotes that these equations belong to the beam with damage. Force balance and continuity conditions at the junctions can be applied, so the state-vectors of the junctions on the beam side without damage are equal to the state-vectors of the junctions on the beam side with damage, which are given by

$$\mathbf{H}_B \mathbf{a}_B^L = \mathbf{H}_D \mathbf{a}_D^L, \tag{10}$$

and

$$\mathbf{H}_B \mathbf{a}_B^R = \mathbf{H}_D \mathbf{a}_D^R. \tag{11}$$

The relationship between the wave vectors $\mathbf{a}_D^L$ and $\mathbf{a}_D^R$ is given by

$$\mathbf{a}_D^R = \mathbf{T}_D \mathbf{a}_D^L, \tag{12}$$

where $\mathbf{T}_D$ is the wave transmission matrix for the damage of the beam and is given by

$$\mathbf{T}_D = \begin{bmatrix} \exp\left(k_{fD} l_D\right) & 0 & 0 & 0 & 0 & 0 \\ 0 & \exp\left(\mathrm{j} k_{fD} l_D\right) & 0 & 0 & 0 & 0 \\ 0 & 0 & \exp\left(\mathrm{j} k_{lD} l_D\right) & 0 & 0 & 0 \\ 0 & 0 & 0 & \exp\left(-k_{fD} l_D\right) & 0 & 0 \\ 0 & 0 & 0 & 0 & \exp\left(\text{-}\mathrm{j} k_{fD} l_D\right) & 0 \\ 0 & 0 & 0 & 0 & 0 & \exp\left(\text{-}\mathrm{j} k_{lD} l_D\right) \end{bmatrix}, \tag{13}$$

where k_{lD} is the longitudinal wavenumber and k_{fD} is the flexural wavenumber of the beam with damage. Combining equations (10-12) gives

$$\mathbf{H}_B \mathbf{a}_B^R - \mathbf{H}_D \mathbf{T}_D \mathbf{H}_D^{-1} \mathbf{H}_B \mathbf{a}_B^L = 0. \tag{14}$$

This is a relationship between the waves either side of the damage. It can be rearranged to group the waves into incoming and outgoing waves, to obtain a simplified system given by

$$\mathbf{a}_{out} = -\mathbf{C}^{-1}\mathbf{B}\mathbf{a}_{in}, \tag{15}$$

where the vectors of wave amplitudes are given by

$$a_{in} = \begin{Bmatrix} A_{R1} \\ A_{R3} \\ A_{Rl} \\ A_{L2} \\ A_{L4} \\ A_{Lr} \end{Bmatrix} \quad \text{and} \quad a_{out} = \begin{Bmatrix} A_{L1} \\ A_{L3} \\ A_{Ll} \\ A_{R2} \\ A_{R4} \\ A_{Rr} \end{Bmatrix},$$

and the matrices $\mathbf{B}$ and $\mathbf{C}$ are given by

$$\mathbf{B} = \left[\left(\mathbf{H}_B\right)_1 \middle| \left(\mathbf{H}_B\right)_2 \middle| \left(\mathbf{H}_B\right)_3 \middle| \left(-\mathbf{H}_D\mathbf{T}_D\mathbf{H}_D^{-1}\mathbf{H}_B\right)_4 \middle| \left(-\mathbf{H}_D\mathbf{T}_D\mathbf{H}_D^{-1}\mathbf{H}_B\right)_5 \middle| \left(-\mathbf{H}_D\mathbf{T}_D\mathbf{H}_D^{-1}\mathbf{H}_B\right)_6 \right],$$

and

$$\mathbf{C} = \left[\left(-\mathbf{H}_D\mathbf{T}_D\mathbf{H}_D^{-1}\mathbf{H}_B\right)_1 \middle| \left(-\mathbf{H}_D\mathbf{T}_D\mathbf{H}_D^{-1}\mathbf{H}_B\right)_2 \middle| \left(-\mathbf{H}_D\mathbf{T}_D\mathbf{H}_D^{-1}\mathbf{H}_B\right)_3 \middle| \left(\mathbf{H}_B\right)_4 \middle| \left(\mathbf{H}_B\right)_5 \middle| \left(\mathbf{H}_B\right)_6 \right],$$

where the subscripts 1 - 6 denote the columns of the respective matrices.

As the damage is symmetric there is no scattering between longitudinal and flexural waves and vice versa. An incident longitudinal wave will scatter into reflected and transmitted longitudinal waves as shown in figure 1, and an incident flexural wave will scatter into reflected and transmitted evanescent and propagating flexural waves as shown in figure 2.

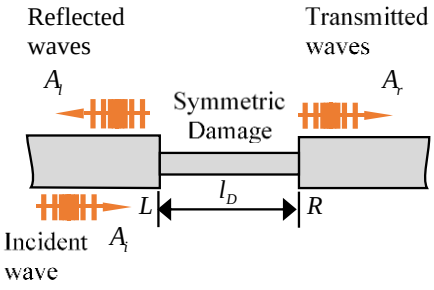

Figure 1. Scattering of longitudinal waves by the symmetric discontinuity.

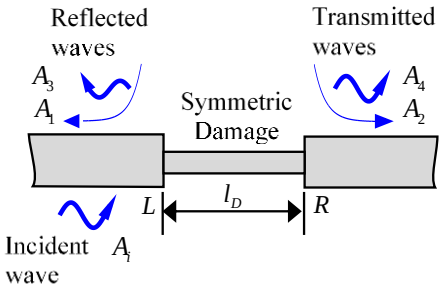

Figure 2. Scattering of flexural waves by the symmetric discontinuity.

Using the model described above the way in which longitudinal and flexural incident waves scatter into reflected and transmitted waves is calculated. The results are shown in figure 3 and 4 respectively, for 0, 10, 30 and 50% of damage. For the longitudinal incident wave, the maximum value of the reflected and the minimum value of the transmitted wave amplitudes is given by

$$\frac{l_D}{\lambda_l} = \frac{2n-1}{4}, \qquad n = 1, 2, 3... \tag{16}$$

It can also be seen that the incident wave is totally transmitted when $l_D/\lambda_l = n/2$.

For flexural waves, it can be seen that the maximum reflected wave and the minimum transmitted wave occur for different values of l_D/λ_f , which varies when the damage increases. This is because, in contrast to the longitudinal wave, the flexural wavelength depends on the geometry of the cross-section in the damages section.

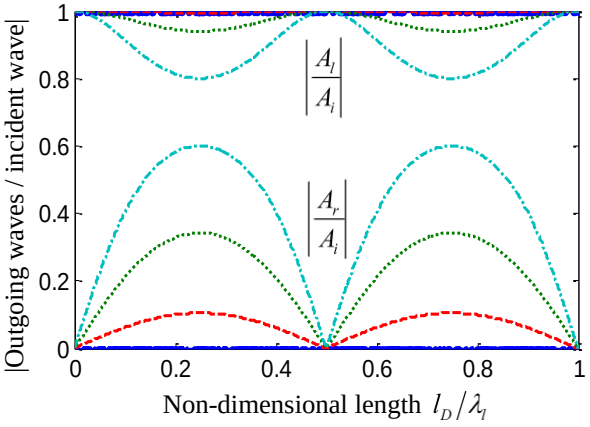

Figure 3. Reflected and transmitted propagating longitudinal waves due to an incident longitudinal wave for different percentages of damage; Solid blue line —, 0% damage; dashed red line ---, 10% damage; thick dotted green line ••••, 30% damage; dashed dot cyan line —•—, 50% damage.

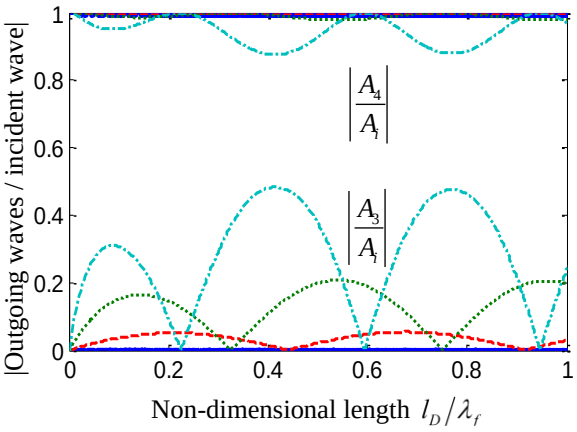

Figure 4. Reflected and transmitted propagating flexural waves due to an incident flexural wave for different percentages of damage; Solid blue line —, 0% damage; dashed red line ---, 10% damage; thick dotted green line ••••, 30% damage; dashed dot cyan line —•—, 50% damage.

4. MODELLING AND TUNING OF PZT ELEMENTS

To launch waves into the structure to determine the structural integrity, PZT elements can be used. They can also be used as sensors as well. Girguiutiu (2008) described the way in which these elements can be tuned to frequencies at which the waves are strongly excited as well as frequencies at which the waves are not excited.

4.1. Piezoelectric actuators

The actuator considered is a bimorph, which uses two PZT elements, one either side of the beam. The either move in-phase and generate longitudinal waves, or move out-of-phase and generate flexural waves. A longitudinal wave actuator is described Brennan et al. (1997), where the generated wave amplitudes are given by

$$\begin{Bmatrix} A_l \\ A_r \end{Bmatrix} = \frac{-\mathrm{j}}{2ESk_l} \begin{bmatrix} 1 & \exp(-\mathrm{j}k_l l_p) \\ 1 & \exp(\mathrm{j}k_l l_p) \end{bmatrix} \begin{Bmatrix} -F \\ F \end{Bmatrix}, \tag{17}$$

where l_p is the length of the PZT elements, and F is related to the voltage applied V_{in} to the PZT elements by (Wang; Rogers, 1990)

$$F = \frac{2Ebd_{31}}{6\hat{h}+\psi} V_{in}, \tag{18}$$

where h is the thickness of the beam, b is the breadth of the beam, $\psi = ES/E_p S_p$ is the stiffness ratio, where E and S is the modulus of elasticity and the cross-sectional area of the beam, E_p and S_p is the modulus of elasticity and the cross-sectional area of the PZT element, $\hat{h} = h_p/h$ is the ratio of the thickness to the PZT element h_p, to the beam, d_{31} is the electromechanical piezoelectric constant.

A flexural wave actuator is described Brennan et al. [10], where the generated wave amplitudes are given by

$$\begin{Bmatrix} A_1 \\ A_2 \\ A_3 \\ A_4 \end{Bmatrix} = \frac{1}{4EIk_f^2} \begin{bmatrix} 1 & \exp(-k_f l_p) \\ -1 & -\exp(k_f l_p) \\ -1 & -\exp(-\mathrm{j}k_f l_p) \\ 1 & \exp(\mathrm{j}k_f l_p) \end{bmatrix} \begin{Bmatrix} -M \\ M \end{Bmatrix}, \tag{19}$$

where M is related to the applied voltage V_{in} to the PZT elements by (Crawley; Anderson, 1990)

$$M = \frac{hEbd_{31}(1+\hat{h})}{6\hat{h}+\psi+12\hat{h}^2+8\hat{h}^3} V_{in}\,. \tag{20}$$

4.2. Piezoelectric sensors

The sensors are two PZT elements perfectly bonded to opposite sides of the beam. With this configuration it is possible to sense separately flexural and longitudinal waves. They are considered to have negligible mass and shear stiffness and the strain is constant across the width of the beam and the sensors.

The relationship between the generated voltage and the axial motion of the beam due to a longitudinal wave is given by Brennan (1994)

$$V_{out} = \frac{d_{31}E_p b_p (u^+(l_p) - u^-(0))}{c}, \tag{21}$$

where c is the capacitance of the sensor and the difference of the displacements at the end of the sensor for a right-going wave when it is located away from the actuator is given by

$$u^+(l_p) - u^-(0) = A_r \left(1 - \exp\left(-\mathrm{j}k_l l_p\right)\right). \tag{22}$$

The relationship between the generated voltage and the lateral motion of the beam due to a flexural wave is given by Brennan (1994)

$$V_{out} = \frac{d_{31}hb_p E_p (w_+'(l_p) - w_-'(0))}{2c}, \tag{23}$$

where the prime denotes the spatial derivate with respect to x. When the sensor is located far from a discontinuity (as is the case in this paper) the relationship between the difference of the slopes at the end of the sensor and a right-going propagating wave is given by

$$w_+'(l_p) - w_+'(0) = jk_f A_4 \left(1 - \exp\left(-\mathrm{j}k_f l_p\right)\right). \tag{24}$$

4.3. Beam with actuator and sensors without damage

The beams system without damage is shown in figure 5, where the PZT elements are fitted to an infinite uniform beam. The PZT 1 elements work such as both an actuator and sensor, and the PZT 2 elements work such as sensor. The distance between them equal to l.

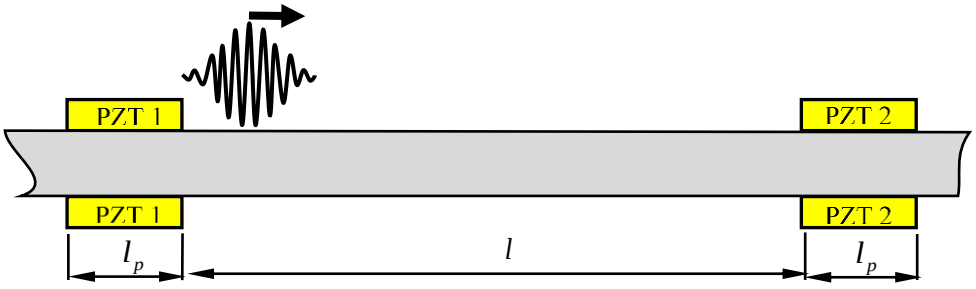

Figure 5. Configuration of the system without damage.

For longitudinal waves the actuator and sensor models can be combined to give the relationship between the response measured by PZT 1 to actuation by PZT 1. It is given by

$$\frac{V_{out}}{V_{in}} = \frac{\mathrm{j}d_{31}^{\,2}E_p b_p}{h_p k_l c(6+\psi)}\left(\exp\left(-\mathrm{j}k_l l_p\right)-1\right), \tag{25}$$

and the corresponding relationship between the response measured by PZT 2 to actuation by PZT 1 is given by

$$\frac{V_{out}}{V_{in}} = -\frac{\mathrm{j}d_{31}^{\,2}E_p b_p}{2h_p k_l c(6+\psi)}\left(\exp\left(-\mathrm{j}k_l l_p\right)-1\right)^2\left(\exp\left(-\mathrm{j}k_l l\right)\right). \tag{26}$$

The input-output relationships are plotted in figure 6 as a function of l_p/λ_l . It can be seen that the largest responses occur when $l_p/\lambda_l = 1/2$, and no responses are registered when $l_p/\lambda_l = 1$.

For flexural waves the corresponding cases for measurement PZT 1 is given by

$$\frac{V_{out}}{V_{in}} = \frac{3d_{31}^{\,2}E_p b_p(1+\hat{d})}{2h_p k_f c\left(6+\psi+12\hat{d}+8\hat{d}^2\right)}\left(1-\left(\exp\left(-k_f l_p\right)\right)-\mathrm{j}\left(1-\left(\exp\left(-\mathrm{j}k_f l_p\right)\right)\right)\right), \tag{27}$$

and for PZT 2 by

$$\frac{V_{out}}{V_{in}} = \frac{3\,\mathrm{j}d_{31}^{\,2}E_p b_p(1+\hat{d})}{4h_p k_f c\left(6+\psi+12\hat{d}+8\hat{d}^2\right)}\left(1-\exp\left(-\mathrm{j}k_f l_p\right)\right)^2\left(\exp\left(-\mathrm{j}k_f l\right)\right) \tag{28}$$

These input-output relationships are plotted as a function of l_p/λ_f in figure 7. Again, it can be seen that there are problems when the sensor or actuator is multiple integer of a wavelength. In the flexural case it can be seen that there are differences between the measurements at PZT 1 and PZT 2 at these frequencies, and this is due to the near-field waves being present at PZT 1 but not at PZT 2.

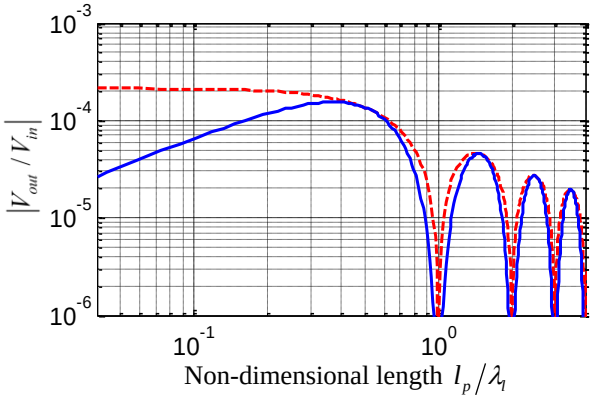

Figure 6. Influence of l_p/λ_l on the Voltage ratio for longitudinal waves; dashed red line ---, sensor 1 located at the left side of the beam (same side of the actuator); Solid blue line —, sensor 2 located at the right side of the beam.

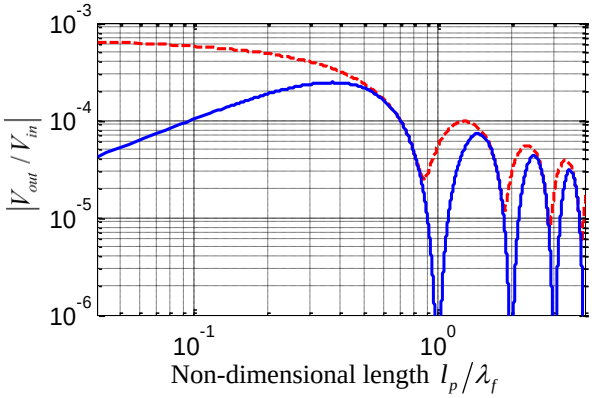

Figure 7. Influence of l_p/λ_f on the Voltage ratio for flexural waves; dashed green line ---, sensor 1 located at the left side of the beam (same side of the actuator); Solid blue line —, sensor 2 located at the right side of the beam.

5. DETECTION AND QUANTIFICATION OF DAMAGE IN THE TIME DOMAIN

To carry out simulations in the time domain the models for the actuators and sensors have to be coupled with the model for the damage discussed previously. The model is assembled in the frequency domain which is then transformed into the time domain using the inverse Fourier transform.

Figure 8 shows two configurations usually used for detecting damage, where the outgoing wave generated by PZT 1 (black wave packet) is used for both cases. In the pulse echo configuration PZT 1 are used as both an actuator and a sensor to detect the reflected waves from the damage (blue wave packet). In the pitch-catch configuration PZT 1 is used as the actuator and PZT 2 is used as sensor to detect the wave transmitted past the damage.

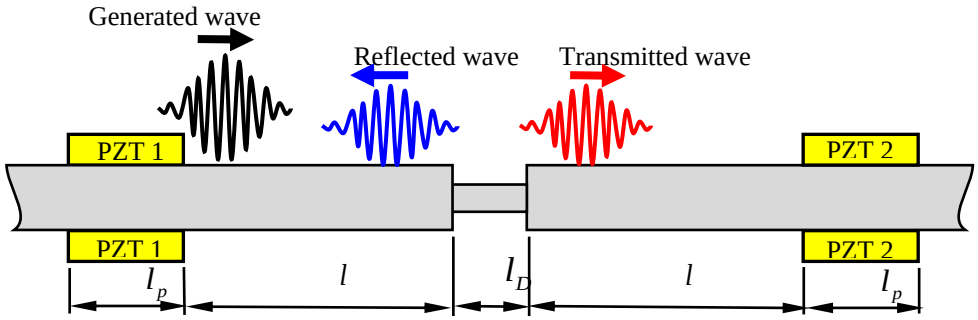

Figure 8. Configuration of the system with damage.

5.1. Analysis in time domain

The complete model is more complex, especially in the time domain, but it can be used to conduct simulations to investigate the effect of damage on the reflected and transmitted waves (Zhongqing; Lin, 2009). For longitudinal waves the system is excited by a burst tone of carrier frequency 100 kHz with longitudinal wavelength $\lambda_l = 0.051\,\text{m}$. The length of the PZT elements is set to $l_p = 0.0256$ m, the length of the damage $l_D = 0.013\,\text{m}$ and distance between the PZT elements and the damage is set to $l = 0.398\,\text{m}$. The values were chosen so that there could be an optimum response of the system with the ratios $l_D/\lambda_l = 1/4$ and $l_p/\lambda_l = 1/2$.

Figure 9 shows the response in time domain for the PZT 1 elements (in a pulse echo configuration). It can be seen that the peaks in the reflected waves increase, but keeping the same phase, when the damage increases.

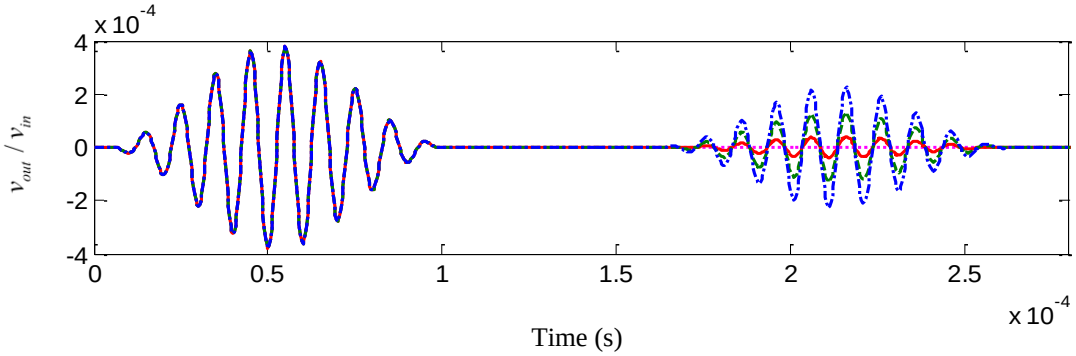

Figure 9. Simulation of Pulse echo configuration due to an incident propagating longitudinal wave with optimal values of the system, for various percentages of symmetric damage; dotted magenta line ••••, 0% damage; thick solid red line —, 10% damage; dashed green line ---, 30% damage; dashed dotted blue line -•-, 50% damage.

Figure 10 shows the response of PZT 2 elements in time domain. This is a pitch-catch configuration. It can be seen that the peaks in the transmitted waves decrease, but keeping the same phase, when the damage increases.

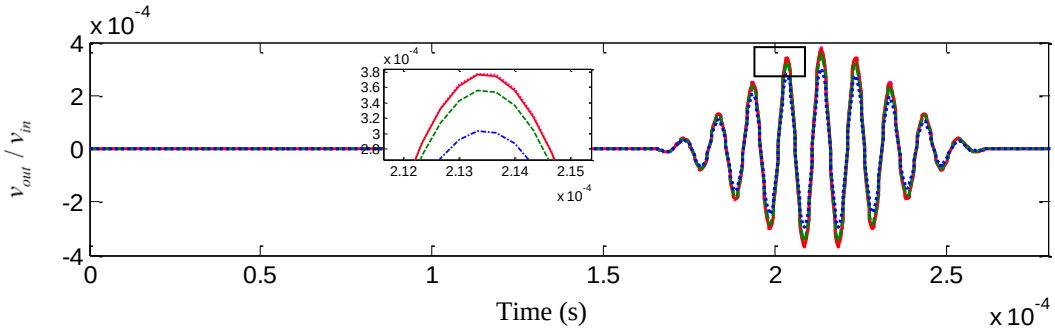

Figure 10. Response in Pitch catch configuration due to an incident longitudinal wave with optimal values of the system, for various percentages of symmetric damage; dotted magenta line ••••, 0% damage; thick solid red line —, 10% damage; dashed green line ---, 30% damage; dashed dotted blue line -•-, 50% damage.

For flexural waves the system is also excited by a burst tone of carrier frequency 100 kHz with flexural wavelength $\lambda_f = 0.014$ m. The length of the PZT elements is set to $l_p = 0.0068$ m, so $l_p / \lambda_f = 1/2$. The length of the damage is set to $l_D = 0.0014$ m, so that there were acceptable responses in each case when the damage varies from 0 to 50% (see Figure 4). The distance between the PZT elements and the damage was set to $l = 0.398$ m as in the longitudinal case.

Figure 11 shows the response in time domain for PZT 1 in a pulse echo configuration. It can be seen that the amplitude of the reflected waves increase as the degree of damage is increased. There is also a small phase shift (see the inset in figure 11), unlike for a longitudinal. This is because the phase velocity for a flexural wave is a function of the geometry of the beam, which changes in the damaged area.

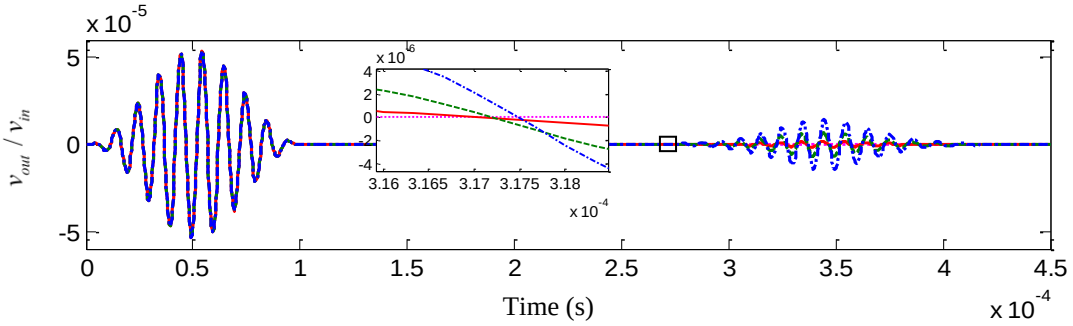

Figure 11. Simulation of Pulse echo configuration due to an incident propagating flexural wave with optimal values of the system, for various percentages of symmetric damage; dotted magenta line ••••, 0% damage; thick solid red line —, 10% damage; dashed green line ---, 30% damage; dashed dotted blue line -•-, 50% damage.

Figure 12 shows the response of PZT 2 in the time domain. This is in the pitch-catch configuration. The dispersive nature of the wave is evident as is the small change in the amplitude as the damage increases. As with the pulse-echo response, the phase shift in the wave packets for different damage levels is evident (see the inset in figure 12)

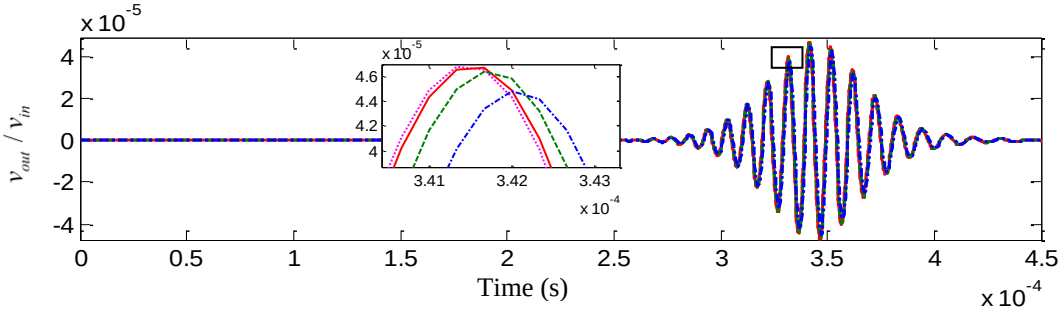

Figure 12. Simulation of Pitch catch configuration due to an incident propagating flexural wave with optimal values for the system, for various percentages of symmetric damage; dotted magenta line ••••, 0% damage; thick solid red line —, 10% damage; dashed green line ---, 30% damage; dashed dotted blue line -•-, 50% damage.

5.2. Quantification

The changes in the measured signals have a particular feature, which can be used to describe the damage. Here, a normalized damage index is used. In the case of the pitch-catch configuration, the normalization is by dividing by the amplitude of the signal without damage. In the case of the pulse-echo configuration, the normalization is by dividing by the amplitude of the signal totally reflected (i.e., 100% damage). The damage index is given by

$$\text{Damage Index} = \frac{\sum_{i=1}^{N} \sqrt{y_i^{\,2}}}{\sum_{i=1}^{N} \sqrt{y_{b(i)}^{\,2}}}, \tag{29}$$

where y_i is the amplitude of the signals correspond to the structure analysed, $y_{b(i)}$ is the amplitude of the baseline and N indicate the number of signals with damage to compare.
To check the conservation of the energy between the reflected and transmitted waves, a power index is also calculated, which is given by

$$\text{Power Index} = \frac{\sum_{i=1}^{N} y_i^{\,2}}{\sum_{i=1}^{N} y_b^{\,2}}. \tag{30}$$

Figure 13 shows the plots of amplitude ratio as a function of the percentage of damage for the pulse- echo (solid blue line) and the pitch-catch configuration (dashed red line) for longitudinal waves. It can be seen that it is better to use the pulse-echo rather than pitch-catch configuration to detect the damage, especially in the range from 0% to 20% of damage. In this range, in the pulse-echo configuration, there is a one-to-one relationship between the ratio of amplitudes and % damage. Figure 14 shows the normalised power in the reflected and transmitted waves as a function percentage of damage of pulse-echo (solid blue line) and pitch-catch configurations (dashed red line). The sum of these is unity for all levels of damage (solid green line).

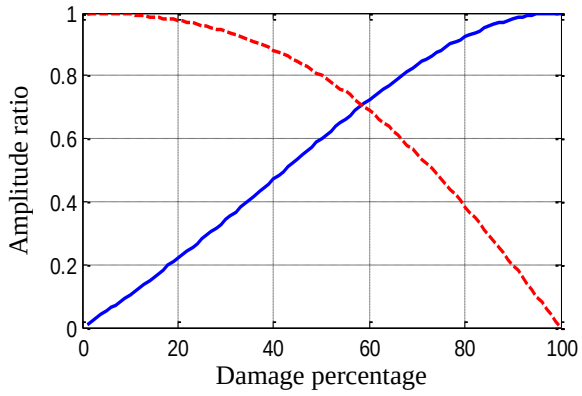

Figure 13. Ratio of Amplitudes vs. Damage percentage, using longitudinal waves and optimal values of the system, for transmitted longitudinal waves, solid blue line — and reflected longitudinal waves, dashed red line --.

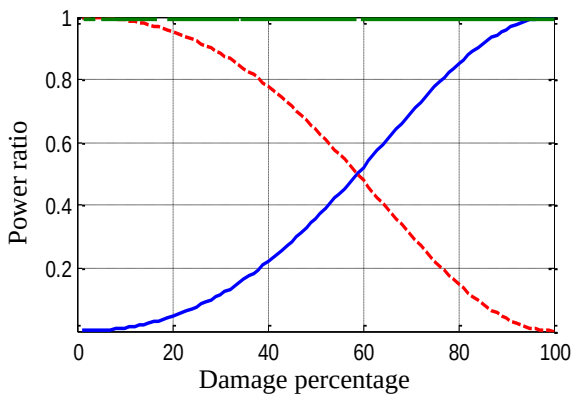

Figure 14. Power ratio vs. Damage percentage, using longitudinal waves and optimal values for the system, for transmitted longitudinal waves, solid blue line —, reflected longitudinal waves, dashed red line --- and total power, solid green line —.

Figure 15 shows the responses of the amplitude ratio as a function of the percentage of damage for the pulse-echo (solid blue line) and the pitch-catch configuration (dashed red line) for flexural waves. It can be seen that it is better to use to pulse-echo rather than pitch-catch to quantify the damage, especially in the range from 0% to 60% of damage. In the pulse-echo configuration, for 0% to 60% of damage the damage is roughly proportional to the amplitude of the reflected wave. There is a trough at about 78% of damage, which is due to the dispersive nature of flexural waves (see figure 4). It is observed that there is a numerical error at a point close to 100% damage due to poor conditioning of the matrices for this condition. As with longitudinal waves energy conservation case, figure 16 shows the normalised power in the

reflected and transmitted waves as a function percentage of damage of pulse-echo (solid blue line) and pitch-catch configurations (dashed red line). The sum of these is unity for all levels of damage (solid green line).

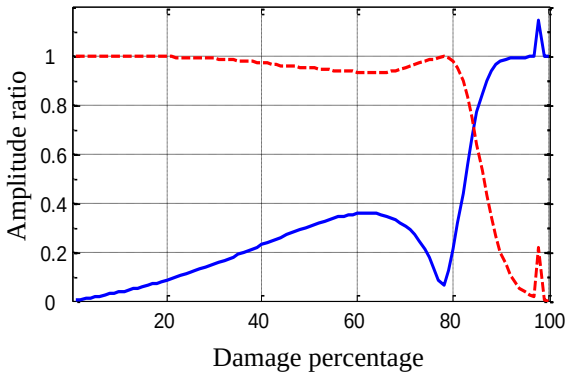

Figure 15. Ratio of Amplitudes vs. Damage percentage, using flexural waves and optimal values for the system, for transmitted waves, solid blue line — and reflected waves, solid red line ---.

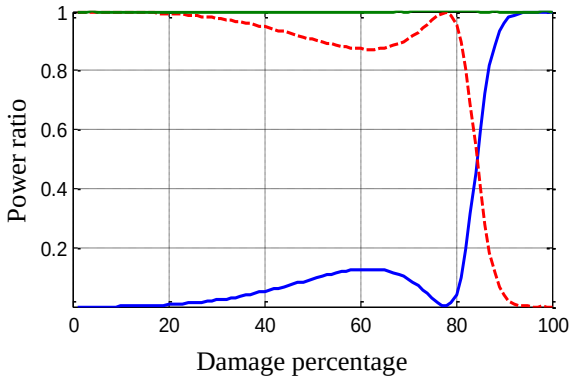

Figure 16. Power ratio vs. Damage percentage, using flexural waves and optimal values for the system, for Transmitted waves, solid blue line —, reflected waves, dashed red line --- and total power, solid green line —.

6. ACKNOWLEDGEMENTS

The authors are thankful to the FAPESP and FAPESPA for financial support.

7. CONCLUSIONS

In this paper the wave approach has been used to investigate the way in which longitudinal waves and flexural waves interact with a damaged section of beam. A frequency domain wave model was developed including PZT actuators and sensors, which was then converted to the time domain numerically using the inverse Fourier transform. The time domain model was used to simulate a situation commonly that commonly occurs in practice, in which a high frequency wave packet is launched into the beam to determine the integrity of the structure. It was found that the longitudinal waves are more sensitive to the damage and that it is better to use the pulse-echo method rather than the pitch-catch method as it is more sensitive to small changes in the beam thickness. Further, it is found that due to the dispersive nature of bending waves, it is possible for the reflected wave amplitude to decrease rather than increase as the beam thickness is reduced.

8. REFERENCES

Brennan, M., 1994. *Active control of waves on one-dimensional structures.* PhD Thesis,University of Southampton, Institute of Sound and Vibration Research.

Brennan, M., Elliot, S., & Pinnington, R., 1997. The dynamic coupling between piezoceramic actuators and a beam. Journal of the acoustical society of America. Vol. 102, pp. 1931-42.

Crawley, E., & Anderson, E., 1990. Detailed models of piezoceramic actuation of beams. Journal Of Intelligent Material Systems & Structures. Vol. 1 pp. 4-25.

Doyle, J., 2009. Guided explorations of the mechanics of solids and structures. Cambridge University.

Fahy, F., Gardonio, P., 2007. Sound and structural vibration. 2. Elsevier. Graff, K., 1975. Wave Motion in Elastic Solids. Clarendon.

Giurgiutiu, V. 2008. Structural Health Monitoring with piezoelectric wafer active sensors. Elsevier.

Mace, B., 1984. Wave reflection and transmission in beams. Journal of Sound & Vibration. Vol. 97, pp. 237-246.

Ostachowicz W., Kudela P., Krawczuk M., & Zak A., 2012. Guided Waves in Structures for SHM. The Time Domain Spectral Element Method. John Wiley & Sons Ltd.

Tenenbaum R., Stutz L., & Fernandes K., 2011. Comparison of vibration and wave propagation approaches applied to assess damage influence on the behaviour of Euler– Bernoulli beams Journal of Computer & Structures. Vol. 89, pp. 1820–28.

Wang, B., & Rogers, C., 1991. Modeling of finite-length spatially distributed induced strain actuators for laminate beams and plates beams. Journal of Intelligent Material Systems & Structures. Vol.2, pp. 238-58.

Zhongqing, S., & Lin, Y., 2009. Identification of Damage Using Lamb Waves: from Fundamentals to Applications. Springer.